Proceedings of the ASME 2018 37th International Conference on Ocean, Offshore and Arctic Engineering
OMAE2018
June 17-22, 2018, Madrid, Spain

OMAE2018-77771

REPRODUCTION OF FREAK WAVES USING VARIATIONAL DATA ASSIMILATION AND OBSERVATION

Wataru Fujimoto [1]
MS&AD InterRisk Research & Consulting, Inc.
Chiyoda-ku, Tokyo, Japan
Email: w.fujimoto@ms-ad-hd.com

Takuji Waseda
Department of Ocean Technology Policy and Environment
University of Tokyo
Kashiwa, Chiba, Japan
Email: waseda@k.u-tokyo.ac.jp

ABSTRACT

This study proposes ideas to reproduce freak waves from observational data. The reproduced data will apply to investigations on freak wave impact to offshore structures. Four-dimensional variational method (4DVAR) was used for the freak wave reproduction. Under a dynamical constraint, 4DVAR minimizes the squared error between observation and model prediction by adjusting the initial condition iteratively. This study utilizes the Higher Order Spectral Method (HOSM) to predict the nonlinear wave evolution, which is essential for freak wave generation. Information on wave spectrum estimated beforehand by a wave model is also employed to stabilize the reproduction. To increase convergence speed with fewer efforts of coding, a type of ensemble-based variational method (a4dVar) was adopted. The a4dVar performs perturbed ensemble simulations to evaluate the gradient of the squared error and is easy to parallelize and implement. This paper conducted twin experiments of HOSM+a4dVar data assimilation. HOSM model generated the true state of the uni-directional wave field, and the spatiotemporal wave field was reconstructed from time series of one virtual wave gauge located in the model. It is assumed that the virtual wave gauge detected a freak wave. The estimation accuracy of linear estimation and HOSM estimation were compared.

1. INTRODUCTION

Freak wave is a major issue in the maritime safety [1]. However, spatiotemporal profile data of freak waves are rarely available. The main data source of freak wave observation is buoy or wave gauge which cannot observe three-dimensional freak wave shapes. Stereo camera imaging has been used for freak wave observation [2], but it is difficult to chase freak wave propagation since the stereo cameras are fixed to capture a particular area. The reproduction of freak wave from the observational data will be necessary to reconstruct the spatiotemporal evolution of freak waves from the limited amount of observational data. The reproduced freak waves are utilized for the investigation of freak wave generation mechanisms. There are many discussions of which mechanics generated freak waves in the real ocean, linear phase focusing or modulational instability [3]. The technique for freak wave reproduction, however, is also applicable to other issues such as to identify the cause of ship accidents.

The four-dimensional variational method (4DVAR) applies to reconstruct spatial wave field in the past [4–6]. 4DVAR iteratively adjusts the initial condition of a numerical model so that the model prediction fits observational data. A promising numerical model for nolinear wave simulation is the Higher Order Spectral Method (HOSM). HOSM accurately and efficiently solves the Euler equations taking into account the nonlinear wave evolution. HOSM can considers the broad spectral bandwidth and the arbitrary nonlinear order under non-breaking wave assumption. A previous study [8] employed the nonlinear Schrödinger equation (NLS) which describes the modulational instability phenomena, but the spectral bandwidth is limited [7]. Other studies [5,6] a simplified method where the modulational instability is neglected. The the second order harmonics and the nonlinear dispersion relationship of the unidirectional wave [9] are considered in their method. This method has a limitation of the nonlinear order. In the real ocean, however, the spectral bandwidth is broad, and the higher order nonlinearity may affect the wave evolution. The HOSM is thought to be the best option.

However, the previous studies of HOSM wave reconstruction [4–6] used a derivative-free optimization method [10] for the fitting and required a huge number of iterations. The convergence speed is expected to increase if the gradient of the squared error between the model prediction and the

[1] Previous affiliation: Department of Ocean Technology Policy and Environment, University of Tokyo, Kashiwa, Chiba, Japan.

observational data. Using the adjoint method, Aragh and Nwogu (2008) evaluated gradient of the squared error directly, but the nonlinear order was not limited [11]. Moreover, implementing the adjoint method requires laborious coding and parallelization is difficult for the adjoint code. Even worse, HOSM uses the perturbation expansion of the velocity potential and contains a lot of terms if the higher order nonlinearity is considered.

A type of ensemble-based variational method (a4dVar) [12] is applicable for accelerating convergence and reducing efforts of coding. The a4dVar conducts numerical differentiation of the squared error by perturbed ensemble simulations to evaluate the gradient. Parallelization is straightforward and implementation is easier than the adjoint method. The Hessian matrix of the squared error is also obtained from the a4dVar method and make the optimization efficient.

This study also proposes utilization of the power spectrum estimated independently such as the third generation wave model. If the amount of the observational data is small, it is difficult to estimate both of wave amplitude and wave phase from the observation. The information of power spectrum constrains the wave amplitude, and the reproduction can be stabilized.

To demonstrate the basic ideas of the HOSM wave reproduction, this study conducted preliminary twin experiments of the a4dVar+HOSM wave reconstruction method for a uni-directional wave. HOSM simulation generated the true wave field, and the spatiotemporal wave field was reconstructed based on virtual observational data extracted from the model. Then, the reconstructed wave field was compared to the true wave for validation of the proposed method.

2. INTRODUCTION

2.1. COST FUNCTION IN THE 4DVAR APPROACH

4DVAR is one of the optimization methods to find the optimum initial condition for the best fit of the model prediction to the observational data (c.f., [13]). The cost function for the wave reproduction is formulated as below,

$$L(\hat{\boldsymbol{\eta}}_{\mathbf{0}}) = \frac{1}{2}\left\|\tilde{H}(\hat{\boldsymbol{\eta}}_{\mathbf{0}}) - \boldsymbol{y}\right\|^2 + \frac{\alpha}{2}\hat{\boldsymbol{\eta}}_{\mathbf{0}}^{*}\mathbf{D}^{-1}\hat{\boldsymbol{\eta}}_{\mathbf{0}}, \qquad (1)$$

where $\hat{\boldsymbol{\eta}}_{\mathbf{0}}$ denotes the Fourier coefficients of the initial condition represented in the wavenumber space. The number of mode to representing the initial condition can be reduced in the wavenumber space than in the physical space. $\tilde{H}$ is a function which relates the Fourier coefficients $\hat{\boldsymbol{\eta}}_{\mathbf{0}}$ in the wavenumber space to the model prediction $\tilde{H}(\hat{\boldsymbol{\eta}}_{\mathbf{0}})$ by HOSM. This first term in the right hand side is the squared error between the model prediction and the observational data.

The second term on the right-hand side of Eq. (1) is the regularization term that constrains the control variable $\hat{\boldsymbol{\eta}}_{\mathbf{0}}$ around $\mathbf{0}$. Especially, the high wavenumber components are difficult to estimate because the energy is small and the group velocity is slow. Then, the estimation tends to diverge. The regularization term gives a penalty for the divergence of the Fourier coefficients $\hat{\boldsymbol{\eta}}_{\mathbf{0}}$ and stabilizes the estimation. The regularization matrix $\mathbf{D}$ indicates the strength of the penalty for each Fourier coefficients and is a diagonal matrix in this study. It is assumed that different wavenumber components are uncorrelated among each other. The diagonal elements of $\mathbf{D}$ is the variance of each wavenumber components and is chosen to be proportional to the prior information of power spectrum $S(\boldsymbol{k})$, i.e. $\mathrm{diag}(\mathbf{D}) \propto S(\boldsymbol{k})$. $S(\boldsymbol{k})$ can be estimated by other ways such as wave models. The regularization term contains a tuning parameter α.

Assuming the linearity of the system, the solution $\hat{\boldsymbol{\eta}}_{\mathbf{0}}^{\dagger}$ of the cost function minimization without the regularization can be obtained from a condition $\tilde{\mathbf{H}}\boldsymbol{x}_{\mathbf{0}} = \boldsymbol{y}$ and is written as $\hat{\boldsymbol{\eta}}_{\mathbf{0}}^{\dagger} = \tilde{\mathbf{H}}^{+}\boldsymbol{y}$, where $\tilde{\mathbf{H}}$ is the Jacobian matrix of the augmented observational operator $\tilde{H}$. $(\ )^{+}$ means the pseudo-inverse matrix. Without the regularization, the estimated value can be noisy due to small condition number of $\tilde{\mathbf{H}}$. Meanwhile, with the regularization, the solution becomes

$$\hat{\boldsymbol{\eta}}_{\mathbf{0}}^{\dagger} = \left(\tilde{\mathbf{H}}^{\boldsymbol{T}}\tilde{\mathbf{H}} + \alpha\mathbf{D}^{-\mathbf{1}}\right)^{-\mathbf{1}}\tilde{\mathbf{H}}^{\boldsymbol{T}} \qquad (2)$$

from the condition that the gradient of the cost function should be zero. The regularization term improves the condition number of the matrix $\tilde{\mathbf{H}}^{\boldsymbol{T}}\tilde{\mathbf{H}} + \alpha\mathbf{D}^{-\mathbf{1}}$ and make the solution smooth [14].

Small value of the regularization parameter α gives less-biased solution, but the estimation can be unstable due to the small eigenvalue of $\tilde{\mathbf{H}}^{\boldsymbol{T}}\tilde{\mathbf{H}} + \alpha\mathbf{D}^{-\mathbf{1}}$. Large regularization stabilizes the estimation and smooths the solution, but high wavenumber feature will be eliminated. The α should be large enough to give stable solutions but small α gives less-biased solutions. Therefore, the minimum tuning parameter α_{opt}, which gives stable solutions, were adopted while decreasing α=1, 0.5 0.1, 0.05 and so forth. "Stable" means that the solution converge in the optimization and that the cost function decreases monotonically. If α is smaller than the chosen parameter α_{opt}, that implies the solution has diverged, or the cost function has oscillated.

Some previous studies combined wave models and HOSM to estimate freak wave occurrence probability in the real ocean [22–24]. They conducted Monte-Carlo simulation of HOSM due to lack of wave phase information. On the other hand, for deterministic freak wave reproduction, this study enhanced the HOSM+wave model combination, so that wave phase information is retrieved from the observational data. The key is the cost function Eq. (1) where information of power spectrum $S(\boldsymbol{k})$ estimated by wave model, observational data $\boldsymbol{y}$, and wave dynamics $\tilde{H}(\hat{\boldsymbol{\eta}}_{\mathbf{0}})$ are summarized in one formulation. The reduction of the cost function gives the best estimate from those given information.

2.2. Ensemble-based 4DVAR

The gradient of the cost function is written as below,

$$\nabla L = \tilde{\mathbf{H}}^{\boldsymbol{T}}\left(\tilde{H}(\hat{\boldsymbol{\eta}}_{\mathbf{0}}) - \boldsymbol{y}\right) + \alpha\mathbf{D}^{-1}\hat{\boldsymbol{\eta}}_{\mathbf{0}} \qquad (3)$$

where $\boldsymbol{\nabla}$ denotes differentiation by the control variable $\widehat{\boldsymbol{\eta}}_{\boldsymbol{0}}$. $\widetilde{\mathbf{H}}$ is the Jacobian matrix of $\widetilde{H}$. Iterative gradient method such as the conjugate gradient method or quasi-Newton method is utilized to the optimization, and the control variable $\widehat{\boldsymbol{\eta}}_{\boldsymbol{0}}$ updates iteratively. The adjoint method needs the adjoint matrix $\widetilde{\mathbf{H}}^{\boldsymbol{T}}$ to evaluate the gradient (3). However, making a code (adjoint code) requires a lot of efforts of coding for the multiplication of the adjoint matrix $\widetilde{\mathbf{H}}^{\boldsymbol{T}}$ and the misfit $\widetilde{H}(\boldsymbol{\eta}_{\boldsymbol{0}}) - \boldsymbol{y}$. Derivatives of all procedures in the numerical code is necessary and should be inverted in the additional code.

The ensemble-based 4DVAR conducts numerical differentiation of the model prediction $\widetilde{H}$ by perturbed ensemble simulation. By adding some perturbations $\boldsymbol{p}_{\boldsymbol{m}}$ $(m = 1 \ldots N_{ens})$ to the initial condition $\boldsymbol{\eta}_{\boldsymbol{0}}$, the model prediction $\widetilde{H}(\boldsymbol{x}_{\boldsymbol{0}} + \boldsymbol{p}_{\boldsymbol{m}})$ is also perturbed. Here, $\boldsymbol{\delta Y}_{\boldsymbol{m}}$ denotes the perturbation of the model prediction $\boldsymbol{\delta Y}_{\boldsymbol{m}} = \widetilde{H}(\boldsymbol{x}_{\boldsymbol{0}} + \boldsymbol{p}_{\boldsymbol{m}}) - \widetilde{H}(\boldsymbol{x}_{\boldsymbol{0}})$. All the perturbations $\boldsymbol{p}_{\boldsymbol{m}}$ and $\boldsymbol{\delta Y}_{\boldsymbol{m}}$ are combined in matrices $\mathbf{P} = (\cdots \quad \boldsymbol{p}_{\boldsymbol{m}} \quad \cdots)$ and $\boldsymbol{\delta \mathbf{Y}} = (\cdots \quad \boldsymbol{\delta Y}_{\boldsymbol{m}} \quad \cdots)$, their relationship is approximated as

$$\boldsymbol{\delta \mathbf{Y}} = \widetilde{\mathbf{H}}\mathbf{P}. \tag{4}$$

The ensemble method updates the control variable $\boldsymbol{\eta}_{\boldsymbol{0}}$ by linear superposition of the perturbation vectors $\boldsymbol{p}_{\boldsymbol{m}}$. Here, $\boldsymbol{s} \in \mathbb{R}^{N_{ens}}$ is the weighting coefficients of the update, and the initial condition in the next iteration is $\boldsymbol{\eta}_{\boldsymbol{0}} + \mathbf{P}\boldsymbol{s}$. The next initial condition should satisfy the $\boldsymbol{\nabla} L = 0$, therefore,

$$\begin{aligned} &\mathbf{P}^{\mathbf{T}} \nabla L \\ &= \mathbf{P}^{\mathbf{T}} \widetilde{\mathbf{H}}^{\boldsymbol{T}} \left(\widetilde{H}(\widehat{\boldsymbol{\eta}}_{\boldsymbol{0}} + \mathbf{P}\boldsymbol{s}) - \boldsymbol{y} \right) + \alpha \mathbf{P}^{\mathbf{T}} \mathbf{D}^{-1} (\widehat{\boldsymbol{\eta}}_{\boldsymbol{0}} + \mathbf{P}\boldsymbol{s}) \\ &= \boldsymbol{\delta \mathbf{Y}}^{\mathbf{T}} \left(\widetilde{H}(\widehat{\boldsymbol{\eta}}_{\boldsymbol{0}}) + \boldsymbol{\delta \mathbf{Y}}\boldsymbol{s} - \boldsymbol{y} \right) + \alpha \mathbf{P}^{\mathbf{T}} \mathbf{D}^{-1} (\widehat{\boldsymbol{\eta}}_{\boldsymbol{0}} + \mathbf{P}\boldsymbol{s}) \\ &= \mathbf{0} \end{aligned} \tag{5}$$

The equation of the initial condition updating is

$$\begin{aligned} &(\boldsymbol{\delta \mathbf{Y}}^{\mathbf{T}} \boldsymbol{\delta \mathbf{Y}} + \alpha \mathbf{P}^{\mathbf{T}} \mathbf{D}^{-1} \mathbf{P}) \boldsymbol{s} \\ &= \boldsymbol{\delta \mathbf{Y}}^{\mathbf{T}} \left(\boldsymbol{y} - \widetilde{H}(\boldsymbol{\eta}_{\boldsymbol{0}}) \right) - \alpha \mathbf{P}^{\mathbf{T}} \mathbf{D}^{-1} \widehat{\boldsymbol{\eta}}_{\boldsymbol{0}}. \end{aligned} \tag{6}$$

The only unknown variable is the weighting coefficient $\boldsymbol{s}$ after the perturbed ensemble simulation, and then Eq. (4) can be solved. $\boldsymbol{\delta \mathbf{Y}}^{\mathbf{T}} \boldsymbol{\delta \mathbf{Y}}$ is the square matrix of dimension $N_{ens} \times N_{ens}$ and is not very large. The ensemble method avoids deriving the adjoint $\widetilde{\mathbf{H}}^{\boldsymbol{T}}$ explicitly.

The choice of perturbation modes is crucial for the convergence speed of the a4dar. The original papers on a4dVar utilized EOF mode of the model trajectory or the misfit $\boldsymbol{y}_{\boldsymbol{t}} - H_t(\widehat{\boldsymbol{\eta}}_{\boldsymbol{t}})$ [15–17]. For the wave reproduction problem, the EOF mode of the wave data is likely close to the Fourier modes. This study proposed to use Fourier modes whose wavenumber is around the peak of the power spectrum of the misfit. The amplitude of the chosen modes should be small enough to ensure the linear approximation Eq. (4) of the $\widetilde{H}(\boldsymbol{\eta}_{\boldsymbol{0}})$ [15–17]. Here, the amplitude was set to 1% of amplitude evaluated from the estimated power spectrum $S(\boldsymbol{k})$.

2.3. Numerical model

HOSM solves Euler equation with a free surface in infinite depth. Although HOSM cannot consider breaking wave, it uses FFTs and is relatively accurate and fast. HOSM of West et al. [18] version was adopted because it conserves Hamiltonian structure in the third order nonlinearity [19]. Simulations of the third order nonlinear HOSM with random wave phase were conducted to spawn a freak wave by taking account of the third order nonlinearity. The power spectrum of the initial waves was JONSWAP spectrum with the peakedness factor $\gamma = 3.3$ and steepness $H_{m0}\, k_p/2 = 0.11$. $k_p = 2\pi/\lambda_p$ is the peak wavenumber where λ_p is the peak wave length. This sea condition is relatively severe compared to an analysis on spectral parameters of the real sea [20]. The spatial domain length was $128\lambda_p$ which is large enough to mitigate effects of periodic boundary condition assumed in HOSM. The duration of time integration was $50T_p$ with the nonlinear spin-up $5T_p$ [21].

The nonlinear spin-up technique is useful for keeping the physical consistency. The analyzed wave started from a linear wave and transited to a nonlinear wave by increasing the nonlinear terms in HOSM gradually. The data assimilation window was after the nonlinear spin-up, and the data during the spin-up (5 wave periods in this study) was discarded. This technique needs only to consider free wave amplitude of the initial wave as the control variable and avoids taking account of complicated nonlinear bound wave generation.

For generating observational data for twin experiment, one freak wave was chosen whose crest height is $\eta_{max} = 1.5H_{m0}$. A virtual wave gauge was located in the model so that the gauge registered the freak wave (Figure 1 and the red line of Figure 2). The wave gauge record after the nonlinear spin-up was used as the virtual observational data for the data assimilation. The wave gauge record was contaminated with white Gaussian noise to be the virtual observational data of the twin experiment. The standard deviation of the Gaussian noise was 10% of the standard deviation of the wave gauge record.

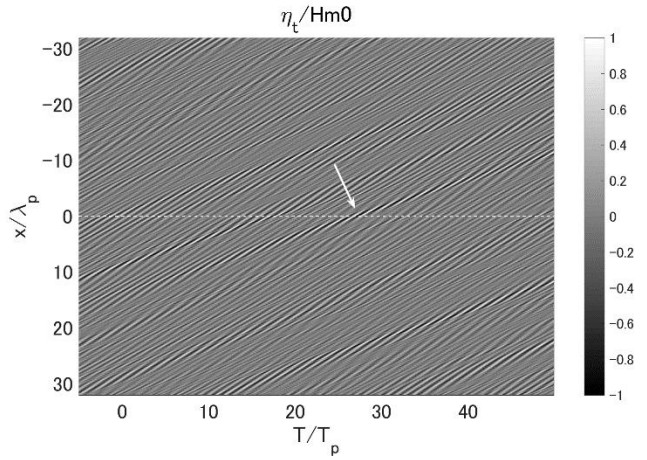

Figure 1 The spatiotemporal profile of the true wave $\boldsymbol{\eta}_{\boldsymbol{t}}$. The wave gauge was located at $\boldsymbol{x} = \mathbf{0}$ (the white broken line). The white arrow indicates the freak wave.

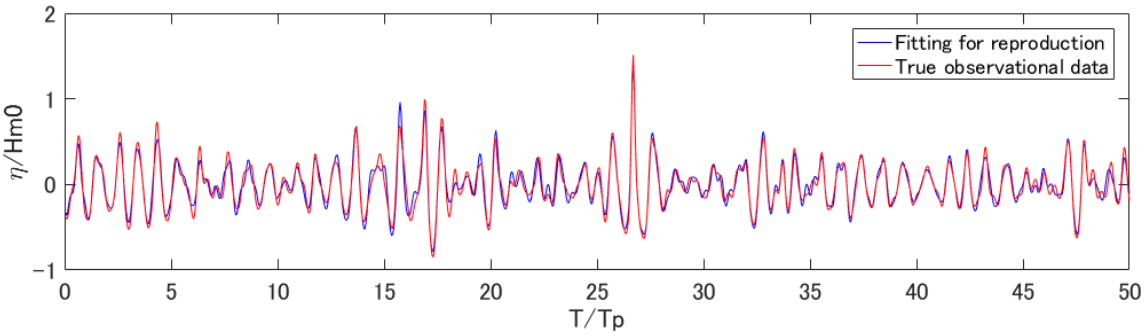

Figure 2 The fitted model prediction ($\tilde{H}(\boldsymbol{\eta_0})$, blue) to the observational data ($\boldsymbol{y}$, red). The freak wave appeared around $T/T_p = 26$.

3. RESULTS

The linear dispersion relationship restricts the size of the domain where the wave field can be reconstructed. The domain is the called "predictable region" [4], and its size is approximated as $\frac{1}{2}C_gT$ where C_g denotes the group velocity and T means the temporal length of the wave gauge data. $T = 50T_p$ in this study, then the size of the predictable region is about $25\lambda_p$. Therefore, the computational domain size for the wave reproduction was $32\,\lambda_p$ to cover this predictable region. Although the predictable region depends on the wavenumber of each component waves, this study considers only the peak wavenumber component for simplicity. The same numerical model, the third order nonlinear HOSM, was used for the wave reproduction as the true wave generation.

The optimization started from the linear estimation which is obtained by assuming the wave is perfectly linear. In the case, $\tilde{H} = \tilde{\mathbf{H}}$ holds, and $\tilde{\mathbf{H}}$ can be derived analytically from the linear dispersion relationship. Then, Eq. (2) gives the optimum initial condition directly without HOSM simulation.

The history of the cost function is shown in Figure 3. The cost function successfully converged in 100 iterations by using 50 ensemble members ($N_{ens} = 50$). $\alpha = 0.005$ was used since this value is the minimum value for the convergence of the cost function. The fitted model prediction to the observational data is shown in Figure 2.

The reconstructed initial wave and the true wave are compared in Figure 4. In the predictable region $x = 0{\sim}25\lambda_p$, the agreement between them was fairly well. The reconstructed wave was attenuated outside of the predictable region due to the regularization.

The nonlinear wave reconstruction using the third order nonlinear HOSM improved the reconstruction quality from the linear estimation. The *freak wave group* was around $x/\lambda_p = 16$ initially ($T/T_p = -5$) and generated the freak wave observed by the wave gauge $x/\lambda_p = 0$ at $T/T_p = 26$ (Figure 1 and Figure 2). The estimation around the freak wave group was poor in the linear reconstruction (Figure 4). However, the nonlinear reconstruction estimated the initial shape of the freak wave group rather precisely.

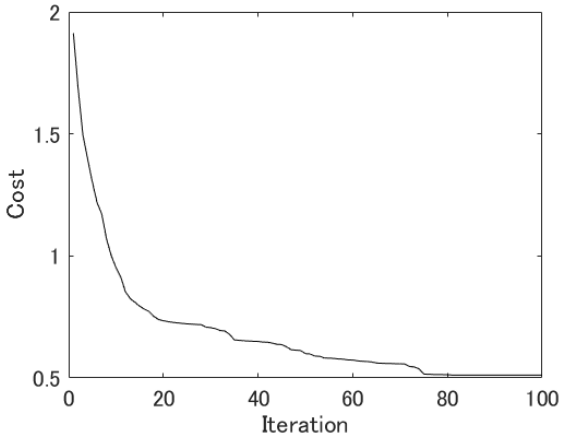

Figure 3 The history of the cost function in the case of the uni-directional wave.

4. CONCLUSION

This study illustrated the basic ideas of the freak wave reconstruction from observational data. The wave reconstruction needs a numerical model to describe the physical process accurately and a reasonable regularization to avoid divergence of reconstruction, especially if the amount of the observational data is limited. HOSM is the best candidate of the numerical model for considering the nonlinear process which possibly cause the freak wave in the ocean. The power spectrum information available from third generation wave models can be reflected to the regularization term.

The a4dVar was employed to invert the observational data to the initial wave field. Implementing the adjoint method is difficult especially for HOSM which has a lot of term originated from the perturbation expansion. Meanwhile, the a4dVar uses the ensemble simulation to conduct numerical differentiation of the cost function and obtains the Hessian matrix for efficient optimization. The a4dVar is suitable for the wave reconstruction by HOSM because implementation and parallelization are easy. The modification of the a4dVar was also proposed in this study. Instead of EOF modes used in the original studies, the Fourier mode was used for giving the perturbed ensembles. This study

demonstrated the performance of HOSM+a4dVar wave reconstruction in the twin experiment using a wave gauge data. Considering the nonlinearity in HOSM was crucial to estimate the freak wave accurately.

Topics for the future works are summarized as the following.

- Robustness of the proposed method to the noise
- Effect of number of ensemble members to the convergence speed
- Extension for the multi-directional wave
- Test for reproducing freak waves which are actually observed in the real ocean
- Utilization of other observational instruments
- More efficient optimization method

The expansion for taking account of other physical processes (such as wind forcing, dissipation, and current) might be necessary for rapidly developing wave field (young wave age) or wave fields in strong current shear. The opposing current amplifies the nonlinear modulation instability [25–27], and the kurtosis increases in rapidly developing wave field by strong wind [28]. Future works should include modeling of those physics to HOSM [29–31].

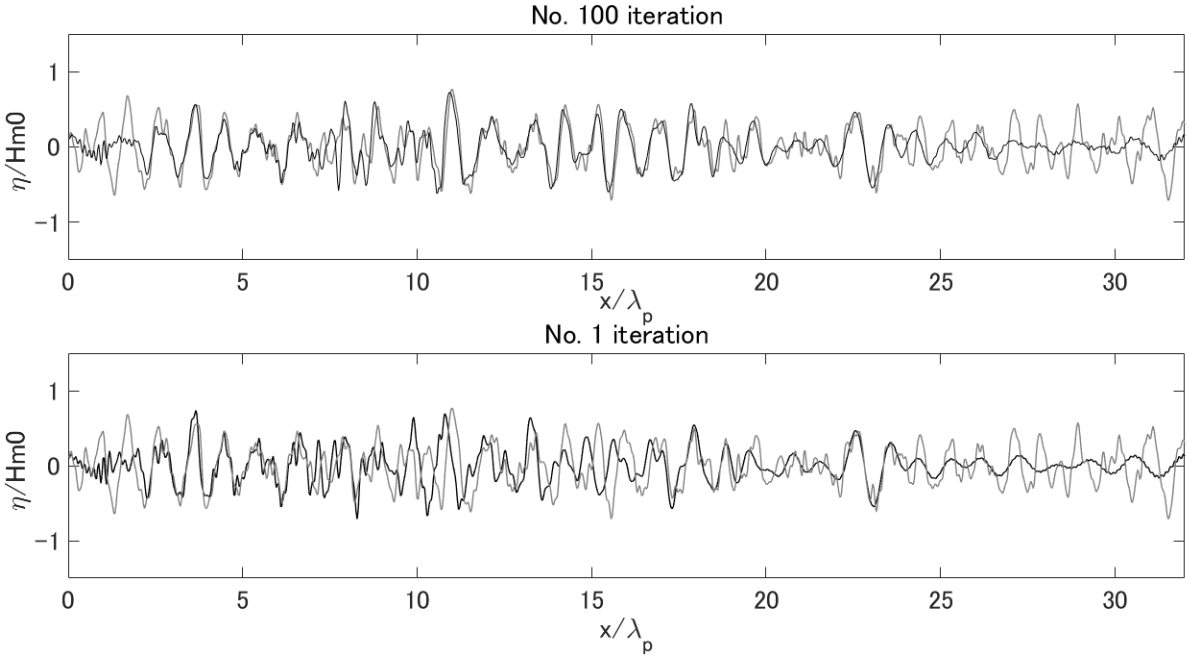

Figure 4 The analysis value (black) of the initial wave. The gray lines show the true wave fields. The upper figure shows the reconstructed wave by nonlinear HOSM+a4dVar assimilation. The lower figure shows the linear reconstruction result.

ACKNOWLEDGEMENTS

Alessandro Toffoli (University of Melbourne) provided the original HOSM code that we modified and used. Max Yaremchuk (Naval Research Laboratory) gave us valuable comments on a4dVar implementation.

REFERENCES

[1] Kharif, C., and Pelinovsky, E., 2003, "Physical Mechanisms of the Rogue Wave Phenomenon," Eur. J. Mech. - B/Fluids, **22**(6), pp. 603–634.

[2] Benetazzo, A., Ardhuin, F., Bergamasco, F., Cavaleri, L., Guimarães, P. V., Schwendeman, M., Sclavo, M., Thomson, J., and Torsello, A., 2017, "On the Shape and Likelihood of Oceanic Rogue Waves," Sci. Rep., **7**(1), p. 8276.

[3] Janssen, P. A. E. M., 2003, "Nonlinear Four-Wave Interactions and Freak Waves," J. Phys. Oceanogr., **33**(4), pp. 863–884.

[4] Wu, G., 2004, "Direct Simulation and Deterministic Prediction of Large-Scale Nonlinear Ocean Wave-Field," Massachusetts Institute of Technology.

[5] Blondel-Couprie, E., Bonnefoy, F., and Ferrant, P., 2010, "Deterministic Non-Linear Wave Prediction Using Probe Data," Ocean Eng., **37**(10), pp. 913–926.

[6] Blondel-Couprie, E., Bonnefoy, F., and Ferrant, P., 2013, "Experimental Validation of Non-Linear Deterministic Prediction Schemes for Long-Crested Waves," Ocean Eng., **58**, pp. 284–292.

[7] Zakharov, V. E., 1968, “Stability of Periodic Waves of Finite Amplitude on the Surface of a Deep Fluid,” J. Appl. Mech. Tech. Phys., **9**(2), pp. 190–194.
[8] Slunyaev, A., Pelinovsky, E., and Guedes Soares, C., 2013, “Reconstruction of Extreme Events Through Numerical Simulations,” J. Offshore Mech. Arct. Eng., **136**(1), p. 11302.
[9] Longuet-Higgins, M. S., and Phillips, O. M., 1962, “Phase Velocity Effects in Tertiary Wave Interactions,” J. Fluid Mech., **12**(3), p. 333.
[10] Rosenbrock, H. H., 1960, “An Automatic Method for Finding the Greatest or Least Value of a Function,” Comput. J., **3**(3), pp. 175–184.
[11] Aragh, S., Nwogu, O., and Lyzenga, D., “Improved Estimation of Ocean Wave Fields from Marine Radars Using Data Assimilation Techniques.”
[12] Yaremchuk, M., Nechaev, D., and Panteleev, G., 2009, “A Method of Successive Corrections of the Control Subspace in the Reduced-Order Variational Data Assimilation*,” Mon. Weather Rev., **137**(9), pp. 2966–2978.
[13] Bannister, R. N., 2017, “A Review of Operational Methods of Variational and Ensemble-Variational Data Assimilation,” Q. J. R. Meteorol. Soc., **143**(703), pp. 607–633.
[14] Tikhonov, A. N., and Arsenin, V. Y., 1979, “Solutions of Ill-Posed Problems,” SIAM Rev., **21**(2), pp. 266–267.
[15] Panteleev, G., Yaremchuk, M., and Rogers, W. E., 2015, “Adjoint-Free Variational Data Assimilation into a Regional Wave Model,” J. Atmos. Ocean. Technol., **32**(7), pp. 1386–1399.
[16] Yaremchuk, M., Martin, P., Koch, A., and Beattie, C., 2016, “Comparison of the Adjoint and Adjoint-Free 4dVar Assimilation of the Hydrographic and Velocity Observations in the Adriatic Sea,” Ocean Model., **97**, pp. 129–140.
[17] Yaremchuk, M., Martin, P., and Beattie, C., 2017, “A Hybrid Approach to Generating Search Subspaces in Dynamically Constrained 4-Dimensional Data Assimilation,” Ocean Model., **117**, pp. 41–51.
[18] West, B. J., Brueckner, K. A., Janda, R. S., Milder, D. M., and Milton, R. L., 1987, “A New Numerical Method for Surface Hydrodynamics,” J Geophys. Res., **92**(C11), pp. 11803–11824.
[19] Onorato, M., Osborne, A. R., and Serio, M., 2007, “On the Relation between Two Numerical Methods for the Computation of Random Surface Gravity Waves,” Eur. J. Mech. B/Fluids, **26**(1), pp. 43–48.
[20] Bitner-Gregersen, E. M., and Toffoli, A., 2012, “On the Probability of Occurrence of Rogue Waves.,” Nat. Hazards Earth …, **12**(3), pp. 751–762.
[21] Dommermuth, D. G., 2000, “The Initialization of Nonlinear Waves Using an Adjustment Scheme,” Wave Motion, **32**(4), pp. 307–317.
[22] Bitner-Gregersen, E. M., Fernandez, L., Lefèvre, J.-M., Monbaliu, J., and Toffoli, A., 2014, “The North Sea Andrea Storm and Numerical Simulations,” Nat. Hazards Earth Syst. Sci., **14**(6), pp. 1407–1415.
[23] Trulsen, K., Nieto Borge, J. C., Gramstad, O., Aouf, L., and Lefèvre, J.-M., 2015, “Crossing Sea State and Rogue Wave Probability during the Prestige Accident,” J. Geophys. Res. Ocean., **120**(10), pp. 7113–7136.
[24] Fedele, F., Brennan, J., Ponce de León, S., Dudley, J. M., Dias, F., De León, S. P., Dudley, J. M., and Dias, F., 2016, “Real World Ocean Rogue Waves Explained without the Modulational Instability,” Sci. Rep., **6**(27715), pp. 1–11.
[25] Aragh, S., and Nwogu, O., 2008, “Variation Assimilating of Synthetic Radar Data into a Pseudo-Spectral Wave Model,” J. Coast. Res., (Special Issue 52), pp. 235–244.
[26] Onorato, M., Proment, D., and Toffoli, A., 2011, “Triggering Rogue Waves in Opposing Currents,” Phys. Rev. Lett., **107**(18), pp. 1–5.
[27] Toffoli, A., Waseda, T., Houtani, H., Kinoshita, T., Collins, K., Proment, D., and Onorato, M., 2013, “Excitation of Rogue Waves in a Variable Medium: An Experimental Study on the Interaction of Water Waves and Currents,” Phys. Rev. E - Stat. Nonlinear, Soft Matter Phys., **87**(5).
[28] Toffoli, A., Waseda, T., Houtani, H., Cavaleri, L., Greaves, D., and Onorato, M., 2016, “Rogue Waves in Opposing Currents: An Experimental Study on Deterministic and Stochastic Wave Trains,” J. Fluid Mech, **769**(April), pp. 277–297.
[29] Toffoli, A., Proment, D., Salman, H., Monbaliu, J., Frascoli, F., Dafilis, M., Stramignoni, E., Forza, R., Manfrin, M., and Onorato, M., 2017, “Wind Generated Rogue Waves in an Annular Wave Flume,” Phys. Rev. Lett., **118**(14), pp. 1–5.
[30] Guyenne, P., 2017, “A High-Order Spectral Method for Nonlinear Water Waves in the Presence of a Linear Shear Current,” Comput. Fluids, **154**, pp. 224–235.
[31] Liu, Y., Yang, D., Guo, X., and Shen, L., 2010, “Numerical Study of Pressure Forcing of Wind on Dynamically Evolving Water Waves,” Phys. Fluids, **22**(4), pp. 1–4.
[32] Tian, Z., and Choi, W., 2013, “Evolution of Deep-Water Waves under Wind Forcing and Wave Breaking Effects: Numerical Simulations and Experimental Assessment,” Eur. J. Mech. B/Fluids, **41**, pp. 11–22.